Proceedings World Geothermal Congress 2020+1
Reykjavik, Iceland, April - October 2021

From brittle to ductile deformation in the continental crust: Mechanics of crystalline reservoirs and implications for hydrothermal circulation.

Mateo Acosta, Benoit Gibert, and Marie Violay

EPFL ENAC LEMR Station 18, 1015, Lausanne, CH

mateo.acosta@epfl.ch

Keywords: Reservoir Mechanics, Hydrothermal Circulation, Induced Seismicity, HP-HT rock deformation, Brittle-Ductile transition

ABSTRACT

Supercritical Geothermal Systems (SGS) and Enhanced Geothermal Systems (EGS) are virtually unlimited, clean and sustainable, sources of electric power. Aside from the current technology costs, their widespread development has yet been limited mainly due to 1) the difficulties of assessing hydrothermal circulation at depths close to the brittle-to ductile transition (BDT) in the case of SGS and 2) due to induced seismicity during deep reservoir stimulation in the case of EGS.

Here, we present the results of novel laboratory experiments conducted in tri-axial stress conditions under high confining pressure (Pc=100-130 MPa), high temperature (300-1000 °C), and high-fluid pressure (Pf=25-30 MPa) on Westerly Granite (WG) samples. We first studied the mechanics of the BDT through experiments performed on intact WG cylinders (Pc= 130 MPa; T= 600 – 1000 °C) where the porosity and permeability evolution were measured during deformation (Violay et al., 2017). In these experiments, we observe that, at ambient temperatures from 600 to 800 °C the failure mode was brittle and the deformation was dilatant (increase in porosity with increasing deformation). At 900 °C, we observe a transition to compactant behavior (decrease in porosity with increasing deformation) due to an increase in the efficiency of crystal plastic processes but still with an overall brittle failure mode (localized shear fracture formation). Finally, at 1000 °C, the deformation is compactant with an overall ductile failure mode (no strain localization, but pore space reduction and strong evidence of crystal plastic processes). Once the BDT was identified, we studied the mechanics of brittle failure by reproducing EGS thermo-hydro-mechanic conditions (Pc= 100 MPa; T= 300-500 °C, Pf= 0-25 MPa) on saw-cut samples (Acosta et al., 2018). There, we studied the influence of fluid pressure, fluid chemistry, and ambient temperature on fault mechanics of dry, and water-and-argon pressurized samples that were reactivated by reproducing tectonic loading. Such fault reactivation experiments allow for the study of simplified fault systems which reproduce the mechanical behavior of idealized single fractures in EGS reservoirs. At a given effective pressure (Pc-Pf= 100 MPa) and ambient temperature (300°C) we observe that dry experiments fail at lower differential stresses ($\Delta\sigma_0$=250 MPa) than Argon ($\Delta\sigma_0$=300 MPa) and Water pressurized experiments ($\Delta\sigma_0$=360 MPa). When studying experiments run at a higher ambient temperature (500 °C), we observe a temperature weakening of the samples so they fail at lower differential stresses. Such observation has strong implications for hydraulic transport in faults and associated seismicity.

Our results suggest that the presence and nature of fluids present in the brittle crust will influence pre- and post-failure behavior of SGS and EGS reservoir rocks. At the BDT, there is a change between dilatant and compactant deformation of deep reservoir crystalline rocks. This implies that, the deeper the reservoir is located into the BDT, the lower the reservoir permeability. In that case, hydrothermal circulation will be diminished without other applied stimulations. In addition, because shear deformation of fault zones is usually related to dilation and increases in permeability (Kranz et al., 1979), the nature and pressure of fluids found in EGS will have strong influence on the reservoir mechanics. Our results will contribute to feasibility analysis for power extraction in both SGS and EGS across the brittle to ductile domains. Through laboratory experiments, we open the door to the study of coupled mechanical deformation and hydraulic transport properties as a function of depth in the continental crust.

1. INTRODUCTION

In the last decades, the geothermal industry has experienced an exponential development (Bertani, 2016). In particular, shallow geothermal resources (mostly used for space heating and industrial uses) have been identified and are exploited all over the world (Lund et al., 2011). Nevertheless, electric power generation using Earth's heat has not been developed to its full potential mainly due to a lack of knowledge of the underground space. In order to achieve temperatures high enough to allow for electric power production (usually > 150 °C), several approaches are possible. Conventional hydrothermal systems, where existing aquifers are exploited as natural convective heat exchangers are relatively simple to set up and operate. Nevertheless, in many tectonic contexts, such systems are usually not an attractive investment due to the low power output compared to the project risk (Muraoka et al, 2014). In order to reach high enough output power to become attractive investments, geothermal projects need to target large depths (4, 5 km depth) where high temperatures (> 200 -250°C) can be exploited (Figure 1). In addition, high enough heat flow rates are needed to get proper return on investment. If such conditions can be reached, geothermal energy has the potential to become a major actor in the world's energy transition. For it to be possible, Supercritical and Enhanced Geothermal Systems (SGS and EGS) must become a safe and controlled alternative to traditional power sources.

On the one hand, SGS are located in very high geothermal gradient zones, at depths of 3-6 km (i.e. temperatures > 400 C), adjacent to the ductile crust (Figure 1A). At such depths, temperatures and pressures allow for the extraction of supercritical fluids (Figure 1B) which can result in a significant increase of output power compared to EGS and conventional hydrothermal systems. In addition, in geographical contexts where fluid injection and depletion of brittle reservoirs could be problematic (in terms of fluid loss and induced seismicity), SGS are a clear alternative for power production (Muraoka et al., 2014). Nevertheless, the Brittle to Ductile Transition (BDT) in the continental crust has been often associated with a limit for fluid circulation due to the low permeability of rocks that flow in a ductile manner ($k < 10^{-18}$ m^2) (Clauser, 1992, Fischer and Paterson, 1992; Morrow et al., 2001, Manning and

Ingebritsen, 1999). The difficulties associated with the assessment of hydrothermal circulation at depth have, up to this point, limited the development of SGS (Muraoka et al., 2014, Bignall and Carey, 2011, Fridleifsson et al., 2014, Dunn et al., 1987, Violay et al., 2012, 2015, 2017).

On the other hand, EGS are hosted at depths of 2-5 km, in tectonic settings where the geothermal gradient is ~35+-5 °C/km (Figure 1A-B). Such contexts are widespread around the world. Therefore, site independence is one of the main strengths of EGS systems. In such tectonic contexts, the fractured crystalline basement deforms in a brittle manner and hydrothermal circulation is mostly controlled by fractures, faults and joints (Stober and Bucher, 2001, Manning and Ingebritsen, 1999, Clauser, 1992, Rojstaczer et al., 2008). Even if the power extraction capacity of EGS is lower than that of SGS (lower temperature, Figure 1B), a proper operation of such systems can allow for the extraction of high enthalpy fluids in the form of vapor (Figure 1B). When necessary, the fractured reservoirs can be stimulated to become permeable enough and allow high power extraction rates (permeability $k>10^{-16}$ m^2) (Olasolo et al., 2016). Hydraulic stimulations change the stress states at depth and have therefore often been associated with induced seismicity (Majer et al., 2007; Haring et al., 2008, Zhang et al., 2014). Induced seismicity has led to the shut-down of several EGS projects in the last decades (Majer et al., 2007; Haring et al., 2008, Evans et al., 2012, Zang et al., 2014 and references therein), significantly slowing down the development of this promising sector of the geothermal industry.

Notwithstanding the effects of reservoir cooling, it is accepted that in the context of SGS, induced seismicity might not be a relevant problem due to the gap of seismicity associated with the BDT (Muraoka et al., 2014). On the other hand, because EGS can be stimulated to increase reservoir permeability, hydrothermal circulation might not be the main issue for the development of these engineered reservoirs (Held et al., 2014, Zang et al., 2014). In fact, geothermal energy costs are expected to reduce with development of this industry (Tester et al., 2006).

For the safe and controlled development of SGS and EGS, it is of critical importance to understand 1) the hydraulic transport properties of reservoirs located close to the BDT and 2) the mechanics of faulted reservoirs hosting engineered systems in crystalline rocks. Here, through a laboratory approach, in a first stage we reproduce the conditions where continental crustal rocks deform from brittle to ductile domains. Under such conditions, we study the evolution of porosity with ongoing deformation in order to assess the hydraulic transport properties of SGS reservoirs at the BDT (Violay et al., 2017). In a second phase, once the BDT has been identified, we study the mechanics of faulted rocks in the presence of fluids at temperatures and stress conditions representative of EGS. There, we evaluate how fluid-rock interactions can affect induced seismicity and try to upscale the observations to reservoir level.

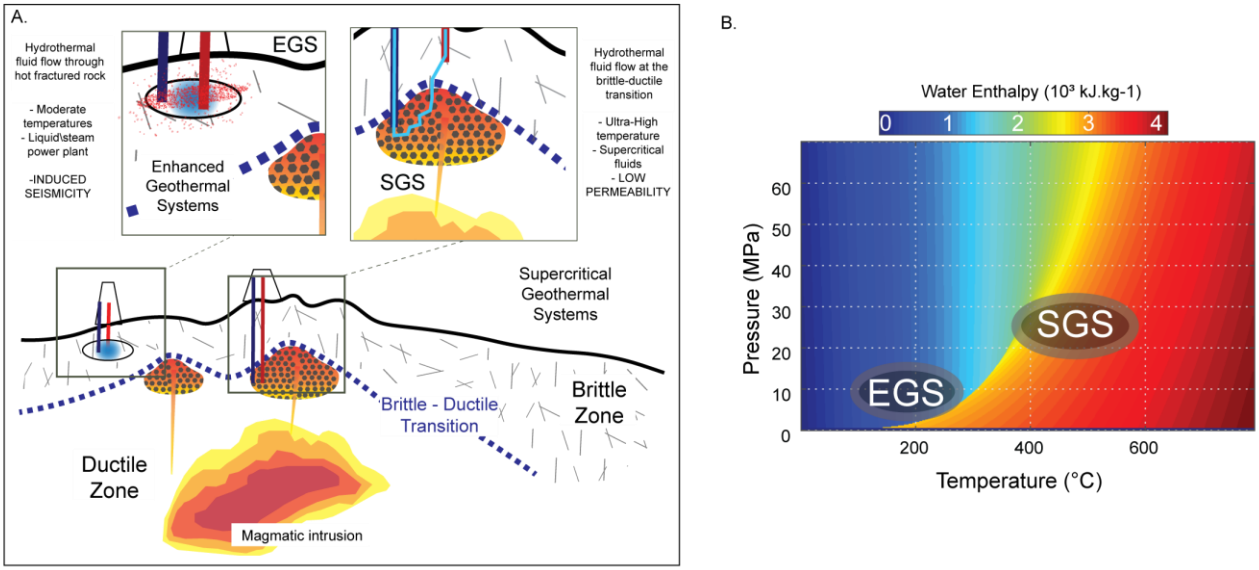

Figure 1: (modified from JBBP): Enhanced and Supercritical Geothermal Systems. A. Sketch and zoom on SGS and EGS in the continental crust. B. Pressure-Temperature diagram of pure water's enthalpy (NIST) showing where SGS and EGS operate.

2. EXPERIMENTAL METHODS

2.1 Starting materials

The experimental samples consisted of Westerly Granite ground cylinders (WG) of ~10 and 15 mm diameter with lengths of 20 and 32 mm for intact and saw-cut deformation respectively. WG is a material that is representative of the upper continental crust (Scholz, 1986) This material is suitable for laboratory work due to its low alteration, low anisotropy, homogeneity, fine grain size and simple mineralogy. The cylinders were heat-treated at 450 °C prior to deformation in order to allow one order of magnitude permeability increase and consequently, reasonable fluid diffusion times across the ground cylinders. Samples of 10 mm diameter were shock cooled in order to enhance the fracture network. Samples of 15 mm diameter were saw-cut at an angle (θ) of 30º to the sample's long axis to create an artificial elliptical fault (~17.3 mm length and ~15 mm width). Fault surfaces were then grinded to ensure perfect contact and roughened with #240 grit paper in order to ensure a minimum cohesion along the fault's interface and impose a constant fault roughness in all specimens.

2.2 Experimental Set-ups.

Experiments were performed on internally heated, gas-medium Paterson-type rigs. The cells can support 700 MPa in confinement and >500 MPa in differential stress for samples of 10 and 15 mm diameter. Fluid pressures (water and argon) were servo-regulated through pressure/volume controllers of 100 MPa maximum capacity (1 mm3 and 10 kPa volume and pressure accuracy). Axial forces were measured through both internal and external load cells and axial displacements (u_{ax}) were recorded through LVDTs located outside or inside the pressurized vessels with an accuracy of ~5 μm.

2.3 Loading Procedure

For water-fluid pressure tests, samples were pre-saturated for a minimum of 48h in an external saturation chamber. Full granite cylinders of 10mm diameter were placed between alumina and zirconia pistons and jacketed with copper or iron depending on the targeted temperature ranging from 600 to 1000 °C. Saw-cut granite samples of 15 mm diameter were placed between alumina pistons and jacketed only with copper in order to work at temperatures ranging from 300 to 500 °C. The assembly was then placed inside a compensated gas pressure vessel, so that measurement of the internal axial force divided by the sample's cross section gives a direct measurement of differential stress $\Delta\sigma = \sigma_1 - \sigma_3$. The confinement was first taken to 5 MPa with no differential stress applied. Then, fluid pressure was increased to 1 MPa until pressure and volume equilibrium were attained at the controller. Then, $\sigma_1' = \sigma_3'$, and (P_f) were taken to the target values (See Table 1 for the experimental details). We denote $\sigma' = \sigma - P_f$ as the effective stress. Finally, axial stress was increased at a constant loading rate resulting in the axial strain rates reported in Table 1. During deformation, (σ_3) and (P_f) were kept constant.

During full cylinder deformation, porosity change of the samples was measured by keeping fluid pressure constant and monitoring the volume change in the pore fluid pressure-volume controller with a resolution of 0.5 mm^3. Porosity variation was corrected for apparatus distortion during axial loading, temperature gradient between pore fluid controller and the sample as detailed in Violay et al. (2017).

In saw-cut sample experiments, the simultaneous increase in a fault's shear stress (τ) and effective normal stress (σ_n') were calculated as:

$$\tau = \frac{\sigma_1 - \sigma_3}{2} * \sin(2\theta)$$

and

$$\sigma_n = \frac{(\sigma_1' - \sigma_3')}{2} * (1 - \cos(2\theta)) + \sigma_3'.$$

The total measured displacement (u_{tot}) was the sum of the elastic displacement of the column (u_{col}), the elastic displacement of the sample (u_{sample}) and the displacement of the fault (u_{fault}). We computed the displacement of the sample and of the fault following the sample's long axis removing the elastic shortening of the column of stiffness (K_{col})~85 kN/mm) as follows:

$$u_{sample} + u_{fault} = \left(u_{tot} - \frac{F_{int}}{K_{col}}\right).$$

Then, we projected the axial displacement to compute the displacement on the fault (u) as:

$$u = \frac{u_{sample} + u_{fault}}{cos(\theta)}.$$

As the samples were saw-cut, most of the sample's deformation took place at the localized shear plane. Therefore, we did not correct our measurements by the 'barreling effect' which is common practice in Paterson-type experiments.

During deformation, part of the applied load was supported by the copper jacket whose rheology is temperature dependent (Frost and Ashby, 1982; Paterson and Wong, 2005; Violay et al., 2017). A correction for the force supported by the copper jacket was therefore applied by considering the assembly as deformable elements in series following the exact same methodology as in Violay et al. 2017. Nevertheless, at temperatures higher than 300 °C, the contribution of the copper jacket to support the internal stress was usually < 1.5 MPa (Bakker, 2016) so that corrections will be plotted as an error bar rather than including them in the mechanical data hereafter.

2.5 Microstructural Analysis

For both full and saw-cut cylinders, 30 μm thick polished thin sections were prepared from each sample and were cut perpendicular to the principal shear planes, along the sample's vertical axis (Figure 2B). Thin sections were further analyzed both under optical microscope (transmitted and polarized light) and under a backscattered mode Scanning Electron Microscope (SEM) using a Phillips XLF-30-FEG and a Zeiss Gemini-SEM 300 with acceleration voltages of 3-8keV (Figure 2C). For saw-cut experiments, a half cylinder was recovered in order to study surface microstructures of the faults under secondary electron mode at 3 keV acceleration voltage (Figure 2D).

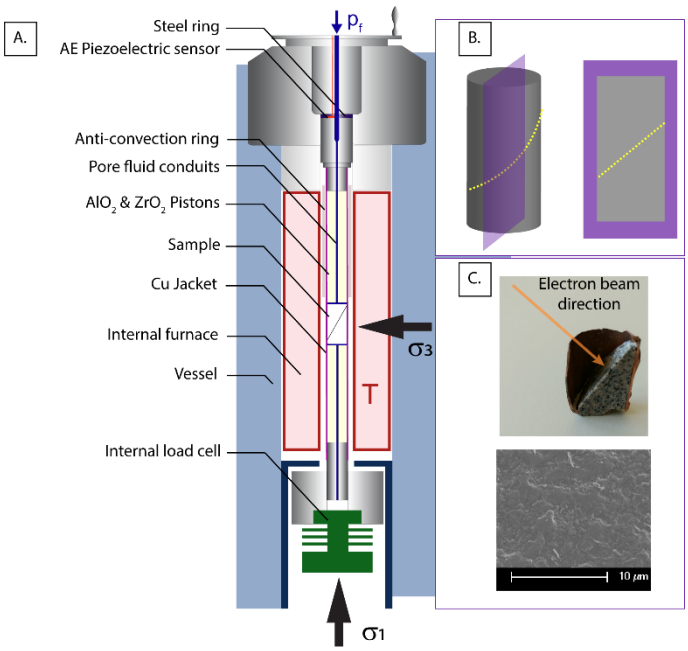

Figure 2: Experimental set-up. A. sketch of the Paterson internally heated triaxial gas apparatus. B. Thin section preparation (the example shown is saw-cut). C. Recovered half saw-cuts are shown next to a scanning electron microscope image of the surface roughness of the samples. (SE mode 3kV acceleration).

3. EXPERIMENTAL RESULTS

We now present the experimental results of mechanical deformation of rock samples. We first present the results on full cylinders at temperatures ranging from 600 °C to 1000 °C. These experiments allow for the identification of the BDT and for the studying of the evolution of porosity during deformation across it. Once the BDT was identified, we proceeded to study the deformation of saw-cut samples in order to study the mechanics of faults in the brittle domain at temperatures ranging from 300 °C to 500 °C.

3.1 Brittle to ductile deformation in full granite cylinders

3.1.1 Mechanical deformation of full cylinders

The deformation of full granite cylinders in terms of differential stress-vs- strain curves is shown in Figure 3A. At all temperatures, deformation was characterized by an initial short (up to <0.1 % axial strain) crack-closure phase with increasing differential stress. Following this, we observed an elastic loading phase where differential stress increased linearly with increments of strain. The elastic loading phase lasted until ~1.5 % axial strain at low temperatures (600 °C – 700 °C) and ~0.2% axial strain at 1000 °C. Once elastic loading finished, all samples presented a strain hardening phase where differential stress increased non linearly with increments of strain up to maximum stresses of ~854 MPa at 600°C, ~436 MPa at 900 °C and ~100 MPa at 1000 °C. When the failure mode was overall fragile (600 °C < T_{amb} < 800 °C), after reaching the peak stress, samples showed a strain softening phase where stress decreased with increments in strain until reaching a residual stress which was fairly constant with increments of strain. The stress drops –defined as the difference between peak and residual stress- decreased with increasing temperature from ~330 MPa at 700 °C to ~150 MPa at 900 °C. At temperatures of 1000°C, the deformation mode was overall ductile (Violay et al, 2017). There, when the maximum stress was reached, the stress was fairly constant with increments of strain.

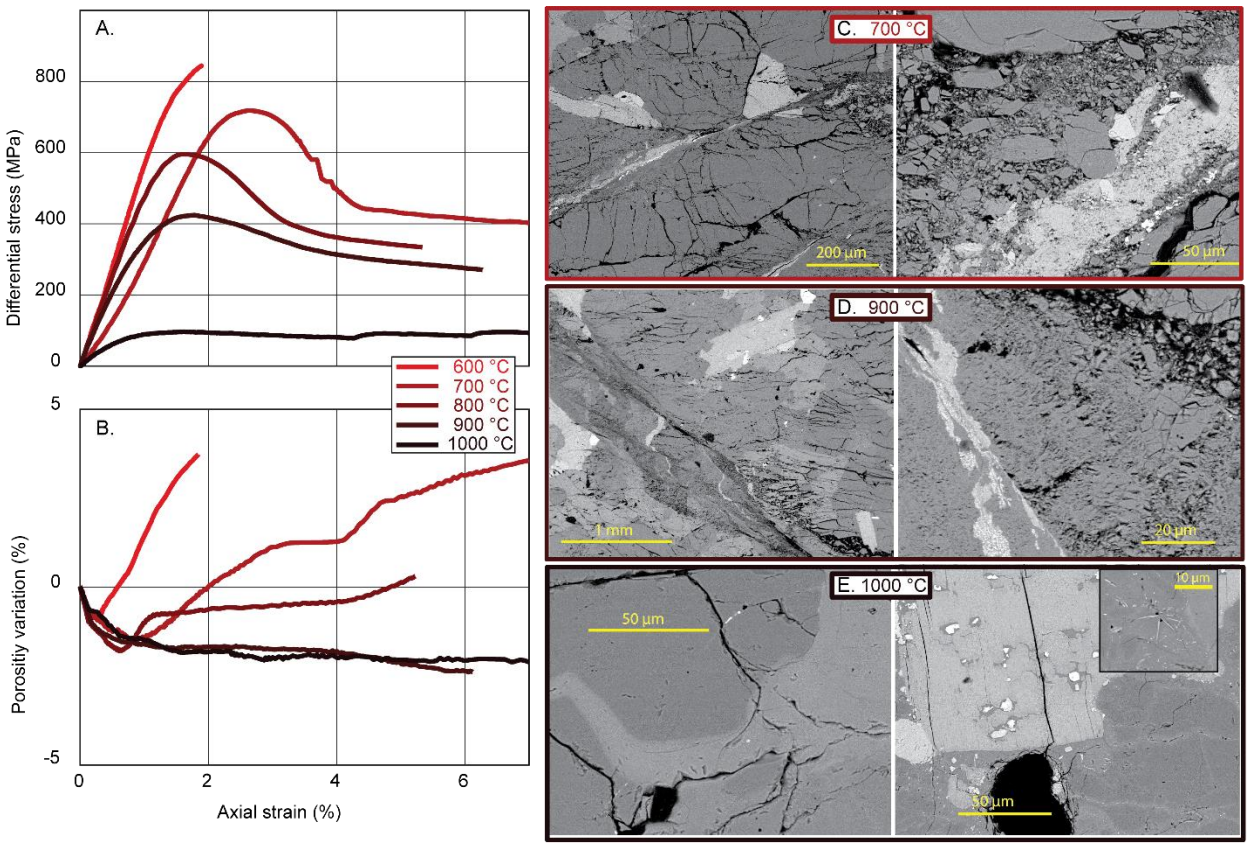

Figure 3: Experimental results of Brittle to Ductile deformation in full granite cylinders. A. Differential stress vs. axial strain for all experiments. B. Porosity variation vs. axial strain during deformation. C-E. Microstructures of the deformed samples, legend shows the experiment. All images were observed under Scanning electron microscope backscattered electron mode of the thin sections.

3.1.2 Porosity evolution during deformation of full cylinders

Using the pore fluid pressure and volume controller, the porosity change during axial deformation of full cylinders was followed in detail and is presented in Figure.3B. At temperatures of 600 – 800 °C porosity first decreased of ~0.5 to 2% until axial strains of 0.3 to 1%. Then, the deformation was dilatant with an increase of porosity of ~4.2 % at 600° and of 1.5% at 800 °C. At temperatures of 900 and 1000 °C, porosity first decreased sharply by ~2% until axial strains of ~1 % before reaching a residual state where porosity variation remained almost constant with increments of axial strain. Overall, the final porosity of failed cylinders was higher than the initial one at temperatures < 800 °C and was lower at temperatures <= 800°C marking a change in deformation mode and hydraulic transport properties with increasing ambient temperature.

3.1.3 Macro and microstructural analysis

The observed macro-structures observed under CT (Violay et al., 2017) show that, at ambient temperatures of 700-900 °C, sample failure was due to strain localization along a single shear fracture traversing the entire sample's length (Figure.3A). In addition, at such temperature, the sample showed little barreling effect. Analysis of the sample's microstructures under SEM and optical microscopy (Figure 3B,C) revealed fine grained (0.1 – 100µm) gouge and densely fractured grains adjacent to the anastomosing shear fractures. Such observations allow us to conclude that the failure mode was mostly brittle. In addition, we found no evidence of crystal plastic processes operating in the bulk sample far from the shear fracture (Figure 3C). At an ambient temperature of 1000 °C, the macrostructure observed by CT showed no evidence of strain localization and no formation of a single shear fracture. At temperatures of 900 and 1000 °C, SEM and optical microscope analysis (Figure.3E,F) show evidence of microcracking (Quartz) and plastic deformation (Quartz undulose extinction and deformation lamellae; Feldspar recrystallization; Biotite kinking and degassing) at the crystal scale. Such microstructures are clear evidence of increased efficiency of crystal plastic deformation processes (Paterson and Wong, 2005).

3.2 Brittle deformation of faulted reservoirs

3..2.1 Fault reactivation of saw-cut samples

The deformation of dry, argon pressurized and water pressurized saw-cut granite cylinders in terms of differential stress vs- axial displacement curves at temperatures of 300 and 500 °C is shown in Figure.4. In all experiments, samples underwent an initial short (up to <0.03 mm displacement) crack-closure phase with increasing differential stress. Then an elastic loading phase followed where differential stress increased linearly with increments of axial displacement. The elastic loading phase lasted until ~0.15 mm axial displacement at all temperatures. Once elastic loading finished, all samples presented a displacement-hardening phase where differential stress increased non linearly with increments of displacement. During this hardening phase, and due to the preexisting weakness plane, the samples are thought to slip in a stable manner rather to accommodate deformation by microcracking or by plastic deformation of rock adjacent to the fault (Scholz et al., 1972). This stable slip phase can in some cases be associated with foreshock

activity. After the precursory slip phase, the samples reached the peak stresses ranging from ~250 to 320 MPa at 300°C, and from ~ 220 to 239 MPa at 500 °C. At this point, the main instabilities (analogs for earthquakes) nucleated and the samples underwent a fast, audible stress drop accompanied by fast slip on the preexisting fault. In our experiments, and due to the high compliance of the axial column, the stress drops were often total, releasing all the stress stored in the fault during co-seismic propagation. Interestingly, at 300 °C we observed that the measured co-seismic slip was again smallest in dry experiments (810 µm) compared to argon (910 µm) and water pressurized (1760 µm) experiments. At 500 °C, the water pressurized experiment presented the largest of all co-seismic slips reaching (9545 µm).

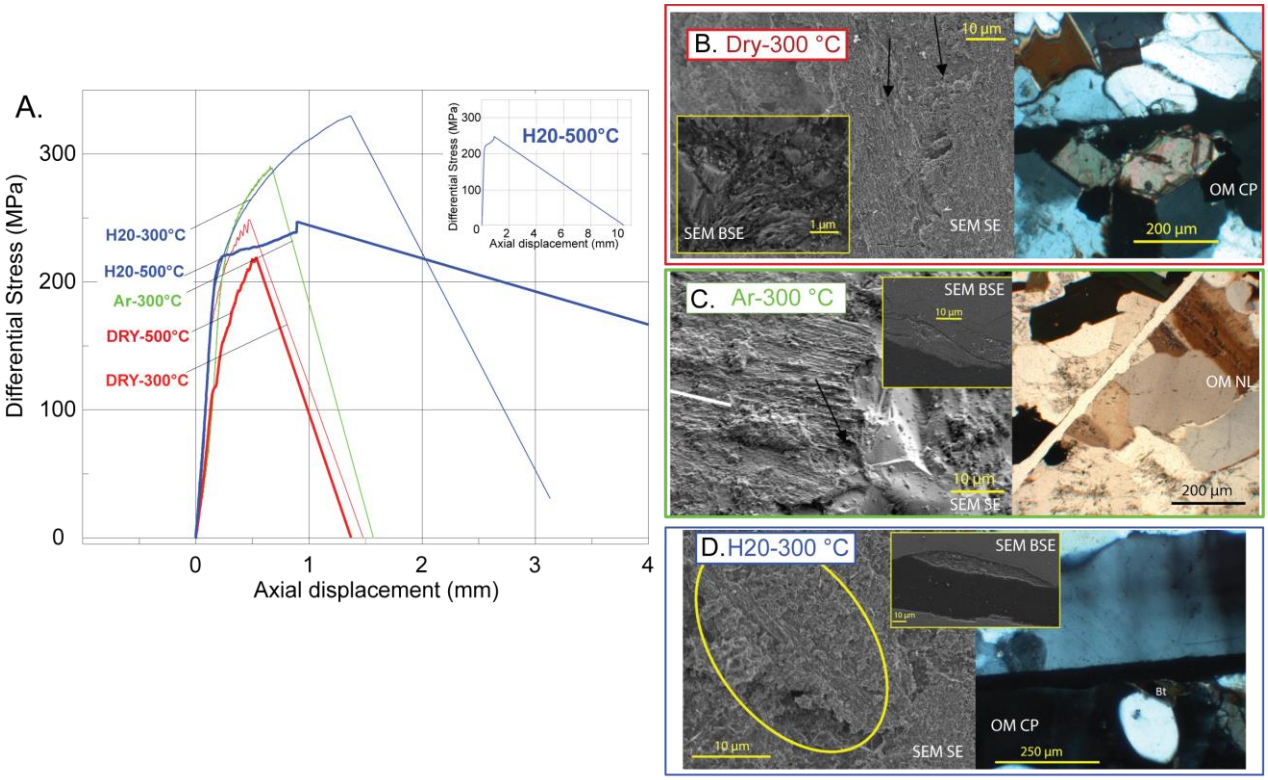

Figure 4: Experimental results of Brittle deformation of saw-cut samples. A. Mechanical results, differential stress vs. axial displacement for experiments performed at 100 MPa effective confinement (25 MPa fluid pressure for all but dry experiments). B-D. Microstructures of the deformed samples, legend shows the experiment. In every image, SEM-BE corresponds to Scanning electron microscope backscattered electron mode observation of thin section. SEM-SE corresponds to Scanning electron microscope secondary electron mode observation of the fault surfaces. OM-CP corresponds to cross polarized optical microscope observation of thin section and OM-NL to direct light observation of thin section.

3.1.3 Microstructural analysis

Optical and Scanning electron microscopy on post-mortem samples are shown in Figure 4B-D. Self-explanatory figure labels show the microstructures corresponding to each experiment.

At all temperatures and under all fluid pressure conditions, we observe a pervasive presence of fine-grained gouge (0.2 to 10 µm) located on the fault's surfaces (Figure4.B-D). At fault boundaries, Qz and KFp grains are highly fractured with fractures oriented both perpendicular and subparallel to the slip direction (Fig 4B). The highly fractured zone has different thicknesses for different experiments ranging from 10 to 200-300 µm in all conditions. In addition, discontinuous patches (~50*50 µm) of glassy material of different thicknesses (~4-6 µm thickness in dry conditions; ~8-24 µm with Argon and 6-12 µm with water pressure) are found all along the slipped faults (Figure 4D). This material is thought to be melted material resulting from fast frictional slip (Lockner et al., 2017; Moore et al., 2017) that stuck to the faults' surfaces upon cooling of the faults after frictional slip arrested. In fact, in Figure 4C-D, we observe that the SEM-SE images of the faults' surfaces often presented ~50*50 µm patches of ropy-like material stretched in the sense of shear (Moore et al., 2017). The thickness of melted patches was determined through OM and SEM-BS of the thin sections perpendicular to the fault. In addition, a verification of these thicknesses was done using SEM-SE change in focus between the highest and lowest melted points observed in the faults surfaces. We observe that the damage zone and melt material thicknesses are larger in the presence of argon compared to dry experiments and the smaller ones are found in water pressurized experiments.

4. DISCUSSION AND IMPLICATIONS FOR DEEP GEOTHERMAL RESERVOIRS

4.1 The Brittle to Ductile transition and its implications for supercritical geothermal systems

Our experimental results have shown that, at confining pressures representative of SGS (~4-6 km depth), the main deformation mode is brittle until temperatures of 800°C at strain rates of 10^{-5} s^{-1} and is mainly ductile at temperatures higher than 1000 °C. Extrapolation of these results to crustal strain rates (10^{-15} s^{-1}; Violay et al., 2017) have shown that the BDT in the continental crust occurs at temperatures lower than those used in these experiments. Such extrapolation using a temperature dependent power law with a temperature gradient of 100°C/km and strain rate of 10^{-14} s^{-1}, predicts that granitic rocks should fail in a brittle mode through strain localization and formation of macroscopic faults at T< 400+-100 °C. On the other hand, at T>400+-100 °C, the deformation mode

should be ductile and likely dominated by crystal plastic processes (Evans et al., 1990). We estimate lower and upper temperature bounds of the BDT in the continental crust to be of 300 and 500 °C respectively (Violay et al., 2017). These results on the porosity evolution of granites during deformation and the corresponding extrapolation to crustal strain rates show that, at ambient temperatures lower than ~300 °C, porosity increases with ongoing deformation. This result has several implications for hydraulic transport properties in crystalline rocks deformed in a brittle manner. In fact, because the deformation is dilatant, deformation of deep reservoir rocks under temperatures lower than that of the BDT should be associated with an increase of permeability of the reservoir (Zoback and Byerlee, 1975). In addition, macroscopic fault systems are usually considered as preferential conduits for fluid flow (Manning and Ingebritsen, 1992; Clauser, 1992). Therefore, in the brittle domain, high fluid extraction capacities for geothermal production are expected following stimulation. On the other hand, at crustal strain rates and temperatures higher than ~500 °C, the overall deformation mode is compactant and associated with a reduction of porosity and permeability of the reservoir rocks. Note that at crustal strain rates and in presence of hydrothermal fluids, an additional reduction of permeability can occur through sealing of rock microcracks (Moore et al., 1994). In the ductile domain, localization of the deformation through macroscopic faults is not expected by definition; further reducing the capacity to circulate fluids and extract heat from the deep (ductile) reservoirs (Violay et al., 2015).

4.2 Brittle deformation of deep fractured crystalline reservoirs and implications for induced seismicity.

At temperatures well below the BDT (here identified ~400+-50 °C), geothermal reservoir rocks are expected to accommodate slow tectonic deformation mostly in a brittle manner. Faults can accommodate large amounts of tectonic deformation over a range of velocities ranging from slow fault slip (some mm/year) or through fast slip events that are earthquakes (tens of cm/s). The main factor that has slowed down the growth of the deep geothermal industry in intraplate continental settings is induced seismicity due to reservoir stimulation (Majer et al., 2007; Haring et al., 2008, Evans et al., 2012, Giardini, 2009; Zang et al., 2014). While seismic and injection data from EGS sites have widely been analyzed (Evans et al., 2012; Zhang et al, 2014), the microphysics of rock/fluid interactions during brittle failure of crustal rocks remain poorly understood and might be helpful for detailed assessment of seismic hazard in EGS sites. Here, building up on previous experimental studies, we analyze the implications of our experimental results for induced seismicity in EGS.

A first striking result from our experiments, is that, at temperatures of 300 and 500 °C granitic faults can be unstable and host large earthquakes. In fact, based on rate-and-state formulation for instability, Blandpied et al. (1998) have shown that granitic fault gouges should only host stable sliding at temperatures higher than 350 °C. The occurrence of instability in our experiments could be due to the high compliance of out apparatus (stiffness of 80 +-5 kN/mm). It is also possible that it is due to the fact that our faults did not host a gouge core. This is for now undetermined. Nevertheless, this is an important result because it calls into question the reasons for the 'seismogenic window' (Scholz, 2019). In fact, it is today accepted that earthquakes can occur in a seismogenic window from 3-4 km to 15 km depth e.g., where the ambient temperatures are in the range of 90 to 350 °C (Scholz, 2019). Our results show that in both dry and wet granite at 500 °C, laboratory faults can present unstable behavior if the slip conditions allow it and if the surrounding medium is compliant enough.

Another important result from these experiments is that fluid-rock interactions during stable sliding and dynamic propagation play a major role in the seismic cycle. In fact, previous studies (Violay et al., 2014, Chen et al., 2017a,b; Urata et al., 2016; Acosta et al., 2018) showed that fault fluid has a cooling effect on the highly-stressed faults' asperities. Therefore, dynamic weakening mechanisms are controlled by thermal interactions between rocks and fluids, thus controlling earthquake propagation. In our experiments, this behavior is confirmed. In dry experiments, the flash heating mechanism (Rice, 2006) can operate from early stages of stable sliding (small precursory slip, u_{prec}), leading to an early instability. In presence of Argon, we have observed that the instability is delayed with respect to dry experiments due to the cooling effect of the fluid. Finally, in presence of water (which has a higher specific heat and density than Argon), the instability is further delayed until enough heat is generated to produce the weakening. (e.g Acosta et al., 2018). This effect is of utmost importance for induced seismicity in EGS because the thermophysical properties of fluids (and therefore their capacity to cool down rocks heated by frictional slip) are highly dependent on a fluid's temperature and pressure. It is easy to imagine, therefore, that the injection of cold-pressurized fluids into the hot rock will strongly change the seismogenic behavior of the reservoir faults and the magnitude of the induced seismic events. Such interactions during fluid injection call for further studies and might help developing safer injection strategies in EGS.

5. APPLICATION TO THE FEASIBILITY OF SGS AND EGS

Supercritical Geothermal Systems target reservoirs at ambient temperatures ranging from 300 to 450 deg C (Muraoka et al., 2014; Bignall and Carey, 2011; Fridleifsson et al., 2014). At these temperatures, rocks are expected to accommodate part of the tectonic deformation through intracrystalline plasticity rather than brittle failure. In our experiments, we have observed 1) that the BDT affects the evolution of porosity (and probably that of permeability) during deformation and 2) that temperature and fluid pressure have a large influence on the mechanical behavior of fault due to thermodynamic effects (e.g Acosta et al., 2018). In light of the experimental results presented in this study, we now evaluate **qualitatively** how the evolution of porosity/permeability and the evolution of fluids thermodynamics with depth affect the reservoir's stored energy and the possible heat flux.

We know that the reservoir's porosity is expected to decrease with increasing deformation (e.g. with the reservoir's maturity, Violay et al., 2017; Moore et al., 1994). We now make a quick estimation of how porosity and permeability affect the stored energy and the heat extraction capacity of and from a geothermal reservoir (DiPippo 2016; Franco and Donatini, 2017). The reservoir's porosity and permeability will directly affect the amount of energy stored in the reservoir and the heat flux extraction capacity for the given reservoir. A first order estimation of the energy stored (E_R) in such geothermal reservoir follows (DiPippo, 2010; Zoback, 2010; Franco and Donatini, 2017):

$$E_R = R_g.\left[\,(1-\phi_R).c_p.\rho.V.(T_R-T_0)+\phi_R.c_{pw}.\rho_w.V.(T_R-T_0)\right].$$

Where R_g is the energy recovery factor of the reservoir (Cataldi R and Muffler P, 1978) defined as the ratio between extractable energy (in terms of current technology, economic conditions, etc...) and the total resource available in the reservoir. ϕ_R is the reservoir's effective porosity, c_p is the rock's specific heat, ρ is the rock's density, V the reservoir's volume, T_R is the reservoir's

temperature, and T_0 is a reference ambient temperature (at the surface for example). Finally, c_{pw} and ρ_w are the water's specific heat and density which strongly depend on temperature and pressure of the reservoir's fluid. From this equation, we highlight two main trends: (1) the energy content increases with increasing temperature as was to be expected and also increases with decreasing porosity. In light of the experimental results presented here, higher temperature reservoirs (> 350 °C) and more mature reservoirs (submitted to larger ductile deformation and so presenting lower porosities) will present the largest energy content. On the other hand, lower temperature reservoirs (< 300 °C) and more mature reservoirs (submitted to larger brittle deformation and so, presenting higher degrees of fracturing and higher porosities) will present the smallest energy contents.

The stored energy content of a reservoir is not the only aspect that should be considered for the feasibility of a geothermal project. In fact, the success of a geothermal project depends mostly on the heat flux that can be extracted from the reservoir up to the surface to be transformed into electricity. A first order estimation of the heat flux that can be extracted can be written:

$$\dot{q_h} = k.\left(\frac{dT}{dz}\right) + \rho_w.c_{pw}.(T_R - T_0).w_f.$$

Here, k is the rock's thermal conductivity and $\frac{dT}{dz}$ is the vertical temperature gradient. Their product defines the conductive heat flow term which can be very small for deep reservoirs. Considering that a heat transfer fluid circulates at a velocity $w_f = \frac{k_{hy}.\rho_w.}{\nu_w}.grad(P)$. through the reservoir, the second term defines a convective heat flow through a length L for a reservoir of permeability k_{hy}. Here, ν_w is the fluid's viscosity. We observe that the permeability and the fluid thermodynamics directly control both the energy content of the reservoir and the heat extraction capacity from the given reservoir.

With this first order analysis, we have observed that (1) porosity greatly affects the stored energy content of the reservoir. (2) if porosity increases with ongoing deformation (brittle deformation, T<300 °C), mature reservoirs will have lower energy contents but higher extraction capacity (due to higher permeability). (3) if porosity decreases with deformation (ductile deformation, T> 350 °C), mature reservoirs will have a much higher energy content but lower heat extraction capacity. All these aspects need to be considered when a deep geothermal reservoir is designed.

6. CONCLUSIONS

In the first part of this study, we investigated the temperatures at which rocks will accommodate deformation by flowing in ductile manner rather than failing in a brittle manner. There, we studied the evolution of hydraulic transport properties of rocks from the continental crust. Once the BDT was identified, we studied the mechanisms of fault reactivation in Brittle faults which are the main control on the mechanical deformation of EGS.

The main conclusions from this study are as follows:

(1) Full granite cylinders fail in a brittle manner forming faults up to temperatures of 800 °C with experimental strain rates (10^{-5} s^{-1}) and at temperatures <300 °C at crustal strain rates (10^{-15} s^{-1}).
(2) Deformation in the brittle domain is associated to an increase in porosity and permeability, which therefore increase the total energy content of brittle reservoirs and heat extraction capacity in geothermal reservoirs.
(3) At temperatures higher than 900°C (at 10^{-5} s^{-1}) and 500 °C (at 10^{-14} s^{-1}) rocks deform in a ductile manner as crystal plastic processes become very efficient.
(4) In the ductile domain, deformation is associated by a decrease in porosity and permeability which could be further decreased due to hydrothermal fluids circulating at depth. Such behavior can decrease the total energy content of deformed reservoirs and can strongly affect the permeability and heat extraction capacity of the reservoir.
(5) Once the BDT was identified, the study of fault mechanics in the brittle domain revealed that fluid thermodynamics has a strong influence on earthquake nucleation and propagation due to thermal interactions with fault rocks.
(6) Thermodynamics of the fluids should have large influence not only on heat extraction from the reservoirs but also on their mechanical behavior.

These results allow for the identification of the BDT in the continental crust and better assessment of hydrothermal circulation through the BDT. The results on brittle fault mechanics in presence of pressurized fluids at realistic stress-pressure and temperature conditions allow considerations for models of induced seismicity.

Acknowledgements

The authors greatly thank N.Marino at Gèosciences Montpellier and L. Gastaldo and B.Frei at EPFL for help with sample preparation and technical assistance during experiments. The authors also thank C.Nevado and D.Delmas for thin section preparation.

5. REFERENCES

Acosta, M., Passelègue, F.X., Schubnel, A. and Violay, M., 2018. Dynamic weakening during earthquakes controlled by fluid thermodynamics. *Nature communications*, ***9***(1), p.3074.

Bakker, R.R., 2016. *Understanding Basement Processes in Sub-Volcanic settings by Laboratory Measurements* (Doctoral dissertation, ETH Zurich).

Bertani, R., 2016. Geothermal power generation in the world 2010–2014 update report. *Geothermics*, ***60***, pp.31-43.

Bignall, G. and Carey, B., 2011, November. A deep (5 km?) geothermal science drilling project for the Taupo Volcanic Zone–Who wants in. In *Proceedings 33rd New Zealand Geothermal Workshop*.

Blanpied, M.L., Lockner, D.A. and Byerlee, J.D., 1995. Frictional slip of granite at hydrothermal conditions. *Journal of Geophysical Research: Solid Earth*, ***100***(B7), pp.13045-13064.

Cataldi R and Muffler P, 1978. Methods for regional assessment of geothermal resources. Geothermics,**7**, 53–89.

Chen, J., Niemeijer, A., Yao, L. and Ma, S., 2017. Water vaporization promotes coseismic fluid pressurization and buffers temperature rise. *Geophysical Research Letters*, ***44***(5), pp.2177-2185.

Chen, J., Niemeijer, A.R. and Fokker, P.A., 2017. Vaporization of fault water during seismic slip. *Journal of Geophysical Research: Solid Earth*, ***122***(6), pp.4237-4276.

Clauser, C., 1992. Permeability of crystalline rocks. *Eos, Transactions American Geophysical Union*, ***73***(21), pp.233-238.

DiPippo, R., 2012. *Geothermal power plants: principles, applications, case studies and environmental impact*. Butterworth-Heinemann.

Dunn, J.C., Ortega, A., Hickox, C.E., Chu, T.Y., Wemple, R.P. and Boehm, R.F., 1987. *Magma energy extraction* (No. SGP-TR-109-3). Sandia National Laboratories (SNL-NM), Albuquerque, NM; University of Utah, Salt Lake City, UT.

NIST Chemistry WebBook, *Thermophysical Properties of Fluid Systems*, **NIST Standard Reference Database Number 69**,Eds. P.J. Linstrom and W.G. Mallard, National Institute of Standards and Technology, Gaithersburg MD, 20899, https://doi.org/10.18434/T4D303, (retrieved June 13, 2019).

Evans, B., Fredrich, J.T. and Wong, T.F., 1990. The brittle-ductile transition in rocks: Recent experimental and theoretical progress. *The Brittle-Ductile Transition in Rocks, Geophys. Monogr. Ser*, ***56***, pp.1-20.

Evans, K.F., Zappone, A., Kraft, T., Deichmann, N. and Moia, F., 2012. A survey of the induced seismic responses to fluid injection in geothermal and CO2 reservoirs in Europe. *Geothermics*, ***41***, pp.30-54.

Fischer, G.J. and Paterson, M.S., 1992. Measurement of permeability and storage capacity in rocks during deformation at high temperature and pressure. In *International Geophysics*, **51**, pp. 213-252. Academic Press.

Franco, A. and Donatini, F., 2017, January. Methods for the estimation of the energy stored in geothermal reservoirs. In *Journal of Physics: Conference Series*,***796***, No. 1, p. 012025. IOP Publishing.

Friðleifsson, G.Ó., Elders, W.A. and Albertsson, A., 2014. The concept of the Iceland deep drilling project. *Geothermics*, ***49***, pp.2-8.

Frost, H.J. and Ashby, M.F., 1982. *Deformation mechanism maps: the plasticity and creep of metals and ceramics*. Pergamon press.

Giardini, D., 2009. Geothermal quake risks must be faced. *Nature*, ***462***(7275), p.848.

Häring, M.O., Schanz, U., Ladner, F. and Dyer, B.C., 2008. Characterisation of the Basel 1 enhanced geothermal system. *Geothermics*, ***37***(5), pp.469-495.

Held, S., Genter, A., Kohl, T., Kölbel, T., Sausse, J. and Schoenball, M., 2014. Economic evaluation of geothermal reservoir performance through modeling the complexity of the operating EGS in Soultz-sous-Forêts. *Geothermics*, ***51***, pp.270-280.

Kato, A., Obara, K., Igarashi, T., Tsuruoka, H., Nakagawa, S. and Hirata, N., 2012. Propagation of slow slip leading up to the 2011 Mw 9.0 Tohoku-Oki earthquake. *Science*, ***335***(6069), pp.705-708.

Kranz, R. L., Frankel, A. D., Engelder, T. & Scholz, C. H. The permeability of whole and jointed Barre Granite. Int. J. Rock Mech. Min. Sci. **16**, (1979) 225–234.

Lockner, D.A., Kilgore, B.D., Beeler, N.M. and Moore, D.E., 2017. The transition from frictional sliding to shear melting in laboratory stick-slip experiments. *Fault zone dynamic processes: Evolution of fault properties during seismic rupture*, ***227***, p.105.

Lund, J.W., Freeston, D.H. and Boyd, T.L., 2011. Direct utilization of geothermal energy 2010 worldwide review. *Geothermics*, ***40***(3), pp.159-180.

Majer, E.L., Baria, R., Stark, M., Oates, S., Bommer, J., Smith, B. and Asanuma, H., 2007. Induced seismicity associated with enhanced geothermal systems. *Geothermics*, ***36***(3), pp.185-222.

Manning, C.E. and Ingebritsen, S.E., 1999. Permeability of the continental crust: Implications of geothermal data and metamorphic systems. *Reviews of Geophysics*, ***37***(1), pp.127-150.

Moore, D.E., Lockner, D.A. and Byerlee, J.D., 1994. Reduction of permeability in granite at elevated temperatures. *Science*, ***265***(5178), pp.1558-1561.

Moore, D.E., Lockner, D.A., Kilgore, B.D. and Beeler, N.M., 2016. *Gallery of melt textures developed in Westerly Granite during high-pressure triaxial friction experiments* (No. 2016-1059). US Geological Survey.

Morrow, C.A., Moore, D.E. and Lockner, D.A., 2001. Permeability reduction in granite under hydrothermal conditions. *Journal of Geophysical Research: Solid Earth*, ***106***(B12), pp.30551-30560.

Muraoka, H., Asanuma, H., Tsuchiya, N., Ito, T., Mogi, T. and Ito, H., 2014. The Japan Beyond-Brittle Project. *Scientific Drilling*, ***17***, pp.51-59.

Olasolo, P., et al.., Enhanced geothermal systems (EGS): A review. *Renewable and Sustainable Energy Reviews*, ***56***, (2016),133-144.

Paterson, M.S. and Wong, T.F., 2005. *Experimental rock deformation-the brittle field*. Springer Science & Business Media.

Rice, J.R., 2006. Heating and weakening of faults during earthquake slip. *Journal of Geophysical Research: Solid Earth*, ***111***(B5).

Rojstaczer, S.A., Ingebritsen, S.E. and Hayba, D.O., 2008. Permeability of continental crust influenced by internal and external forcing. *Geofluids*, ***8***(2), pp.128-139.

Ruiz, S., Metois, M., Fuenzalida, A., Ruiz, J., Leyton, F., Grandin, R., Vigny, C., Madariaga, R. and Campos, J., 2014. Intense foreshocks and a slow slip event preceded the 2014 Iquique Mw 8.1 earthquake. *Science*, ***345***(6201), pp.1165-1169.

Scholz, C., Molnar, P. and Johnson, T., 1972. Detailed studies of frictional sliding of granite and implications for the earthquake mechanism. *Journal of geophysical research*, ***77***(32), pp.6392-6406.

Scholz, C.H., 1986. Preface: A short geophysical history of Westerly granite. *Washington DC American Geophysical Union Geophysical Monograph Series*, ***37***.

Scholz, C.H., 2019. *The mechanics of earthquakes and faulting*. Cambridge university press.

Socquet, A., Valdes, J.P., Jara, J., Cotton, F., Walpersdorf, A., Cotte, N., Specht, S., Ortega-Culaciati, F., Carrizo, D. and Norabuena, E., 2017. An 8 month slow slip event triggers progressive nucleation of the 2014 Chile megathrust. *Geophysical Research Letters*, ***44***(9), pp.4046-4053.

Stober, I. and Bucher, K., Hydraulic properties of the crystalline basement. *Hydrogeology Journal*, ***15***(2), (2007), pp.213-224.

Tester, J.W., Anderson, B.J., Batchelor, A.S., Blackwell, D.D., DiPippo, R., Drake, E.M., Garnish, J., Livesay, B., Moore, M.C., Nichols, K. and Petty, S., 2006. The future of geothermal energy. *Impact of Enhanced Geothermal Systems (EGS) on the United States in the 21st Century, Massachusetts Institute of Technology, Cambridge, MA*, *372*.

Urata, Y., Kuge, K. and Kase, Y., 2015. Effect of water phase transition on dynamic ruptures with thermal pressurization: Numerical simulations with changes in physical properties of water. *Journal of Geophysical Research: Solid Earth*, ***120***(2), pp.962-975.

Violay, M., Gibert, B., Mainprice, D. and Burg, J.P., 2015. Brittle versus ductile deformation as the main control of the deep fluid circulation in oceanic crust. *Geophysical Research Letters*, ***42***(8), pp.2767-2773.

Violay, M., Gibert, B., Mainprice, D., Evans, B., Dautria, J.M., Azais, P. and Pezard, P., 2012. An experimental study of the brittle ductile transition of basalt at oceanic crust pressure and temperature conditions. *Journal of Geophysical Research: Solid Earth*, ***117***(B3).

Violay, M., Heap, M.J., Acosta, M. and Madonna, C., 2017. Porosity evolution at the brittle-ductile transition in the continental crust: Implications for deep hydro-geothermal circulation. *Scientific reports*, ***7***(1), p.7705.

Voss, N., Dixon, T.H., Liu, Z., Malservisi, R., Protti, M. and Schwartz, S., 2018. Do slow slip events trigger large and great megathrust earthquakes?. *Science advances*, ***4***(10), p.eaat8472.

Zang, A., Oye, V., Jousset, P., Deichmann, N., Gritto, R., McGarr, A., Majer, E. and Bruhn, D., 2014. Analysis of induced seismicity in geothermal reservoirs–An overview. *Geothermics*, ***52***, pp.6-21.

Zoback, M.D. and Byerlee, J.D., 1975. The effect of microcrack dilatancy on the permeability of Westerly granite. *Journal of Geophysical Research*, ***80***(5), pp.752-755.

Zoback, M.D., 2010. *Reservoir geomechanics*. Cambridge University Press.